RESEARCH ARTICLE

Pediatric Cystic Fibrosis Sputum Can Be Chemically Dynamic, Anoxic, and Extremely Reduced Due to Hydrogen Sulfide Formation

Elise S. Cowley,[a] Sebastian H. Kopf,[b,c] Alejandro LaRiviere,[a] Wiebke Ziebis,[d] Dianne K. Newman[a,b,c]

Division of Biology and Biological Engineering, California Institute of Technology, Pasadena, California, USA[a]; Division of Geological and Planetary Sciences, California Institute of Technology, Pasadena, California, USA[b]; Howard Hughes Medical Institute, Pasadena, California, USA[c]; Department of Biological Sciences, University of Southern California, Los Angeles, California, USA[d]

ABSTRACT **Severe and persistent bacterial lung infections characterize cystic fibrosis (CF). While several studies have documented the microbial diversity within CF lung mucus, we know much less about the inorganic chemistry that constrains microbial metabolic processes and their distribution. We hypothesized that sputum is chemically heterogeneous both within and between patients. To test this, we measured microprofiles of oxygen and sulfide concentrations as well as pH and oxidation-reduction potentials in 48 sputum samples from 22 pediatric patients with CF. Inorganic ions were measured in 20 samples from 12 patients. In all cases, oxygen was depleted within the first few millimeters below the sputum-air interface. Apart from this steep oxycline, anoxia dominated the sputum environment. Different sputum samples exhibited a broad range of redox conditions, with either oxidizing (16 mV to 355 mV) or reducing (−300 to −107 mV) potentials. The majority of reduced samples contained hydrogen sulfide and had a low pH (2.9 to 6.5). Sulfide concentrations increased at a rate of 0.30 μM H_2S/min. Nitrous oxide was detected in only one sample that also contained sulfide. Microenvironmental variability was observed both within a single patient over time and between patients. Modeling oxygen dynamics within CF mucus plugs indicates that anoxic zones vary as a function of bacterial load and mucus thickness and can occupy a significant portion of the mucus volume. Thus, aerobic respiration accounts only partially for pathogen survival in CF sputum, motivating research to identify mechanisms of survival under conditions that span fluctuating redox states, including sulfidic environments.**

IMPORTANCE **Microbial infections are the major cause of morbidity and mortality in people living with CF, and yet microbial growth and survival in CF airways are not well understood. Insufficient information about the chemistry of the *in vivo* environment contributes to this knowledge gap. Our documentation of variable redox states corresponding to the presence or absence of sulfide begins to fill this void and motivates understanding of how different opportunistic pathogens adapt in these dynamic environments. Given the changing chemical state of CF sputum over time, it is important to consider a spectrum of aerobic and anaerobic lifestyles when studying CF pathogens in the laboratory. This work not only provides relevant constraints that can shape the design of laboratory experiments, it also suggests that sulfide might be a useful proxy for assessing the redox state of sputum in the clinic.**

Received 7 May 2015 **Accepted** 25 June 2015 **Published** 28 July 2015

Citation Cowley ES, Kopf SH, LaRiviere A, Ziebis W, Newman DK. 2015. Pediatric cystic fibrosis sputum can be chemically dynamic, anoxic, and extremely reduced due to hydrogen sulfide formation. mBio 6(4):e00767-15. doi:10.1128/mBio.00767-15.

Invited Editor Alfred Michael Spormann, Stanford University **Editor** David A. Relman, VA Palo Alto Health Care System

Address correspondence to Wiebke Ziebis, wziebis@usc.edu, or Dianne K. Newman, dkn@caltech.edu.

Cystic fibrosis (CF) is an autosomal recessive human genetic disease resulting from mutations in the cystic fibrosis transmembrane conductance regulator (CFTR) gene (1). Mutations in the CFTR gene result in the defective transfer of ions across membranes, impacting many body systems, but most severely the respiratory tract. The loss of ion homeostasis at the respiratory epithelium leads to the presence of a dehydrated, thickened mucosal layer that accumulates and can obstruct the airways as well as limit the motion of the airway cilia. People living with CF are susceptible to chronic lung infection by opportunistic pathogens because of their inability to clear thickened mucus from airways (2, 3). These infections ultimately are responsible for their morbidity and mortality (4–6). CF has been characterized in 70,000 individuals worldwide, with 30,000 residing in the United States and approximately 1,000 new cases of CF diagnosed each year. The population of people living with CF is split nearly evenly between adults and pediatric patients, emphasizing the importance of pediatric CF research (7). CF is characterized by the accumulation of irreversible lung damage, motivating early intervention to prevent disease progression.

The diversity and adaptation of opportunistic pathogens within the CF lung environment are, in part, what render CF infections so difficult to eradicate (8–10). Yet a growing body of research on the stability of microbes in different ecosystems, such as the human gut, indicates that, while diversity at the organismal level can be vast, the metabolic networks that underpin microbial communities are often conserved and constrained by environmental parameters (11). Few studies have attempted to character-

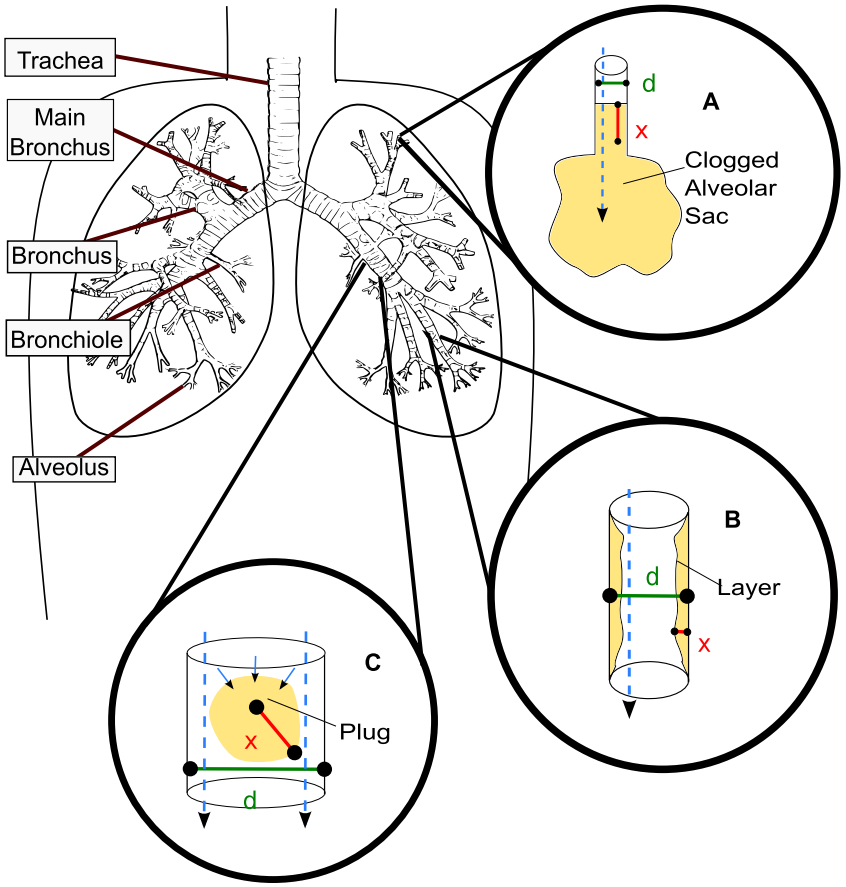

FIG 1 Overview of the respiratory airways. Tan coloring indicates mucus. Cyan dashed arrows indicate the direction of possible oxygen transport. In CF lungs, mucus can aggregate in different scenarios. In each scenario, "d" indicates the diameter of the airway and "x" indicates the mucus thickness. (A) Although less common in CF, the small airways, the alveolar sacs, can clog with mucus entirely ($d \leq 200\ \mu m$). (B) The surface layer of the bronchioles becomes dehydrated, and mucus thickening begins ($300\ \mu m \leq d \leq 1{,}000\ \mu m$). (C) Mucus aggregates can dislodge from lower airways and become lodged in larger, upper airways (the d value depends on the airway the aggregate is dislodged into; $300\ \mu m \leq d \leq 5{,}000\ \mu m$).

ize the *in vivo* chemistry of mucus collecting in CF airways, yet such measurements are essential if we are to understand how microorganisms survive in the lung and impact the microenvironment. Oxygen is a key inorganic substrate whose abundance dictates which metabolisms are utilized. To date, three studies have directly measured the oxygen content in people living with CF. Oxygen measurements completed during bronchoscopies of upper lung lobes of three CF patients demonstrated oxygen depletion in mucopurulent masses (12). Oxygen profiles of 20 CF patients undergoing sinus surgery revealed lower oxygen tension in the mucosa of the sinus, but not the sinus lumen; anoxic conditions were found in 18% of the measured CF sinuses (13). Recently, N_2O and O_2 concentrations were profiled in sputum samples from 7 CF patients; these samples were collected in cylindrical glass vials. Under these sampling conditions, an oxygen gradient near the air-sputum interface was followed by an anoxic zone, in which N_2O accumulated and disappeared over time (14). Amino acids, sugars, salts, phenazines, and iron oxidation states have also been quantified in bulk sputum samples (15–17). Other chemical parameters, including the pH of exhaled breath, have been measured directly from patients (18, 19).

Studies measuring gene expression have shed complementary light on microbial adaptation to environmental changes. While important members of the CF lung community, such as *Pseudomonas aeruginosa*, are sometimes still referred to as "obligate aerobes" (20, 21), it is generally well accepted that they have the capability for microaerobic growth in 3 to 10 μM O_2 (22), as well as for anaerobic growth and survival (16, 21, 23–28). Moreover, several studies have found evidence for the presence of strict anaerobes within CF microbial populations, through both culture-dependent and culture-independent approaches (29, 30). Indeed, a recent metagenomic and metatranscriptomic study of microbial communities in 6 different patients revealed that CF lung pathogens utilize a variety of anabolic and catabolic pathways. For example, CF lung communities expressed enzymes involved in amino acid catabolism, folate biosynthesis, and lipoic acid biosynthesis. In addition to energy generation via fermentative pathways, the data were consistent with catabolism by oxidative phosphorylation using a variety of terminal electron acceptors (31).

Despite appreciation of the metabolic versatility of many CF pathogens, relatively little is known about the variability in redox states between and within patients at the microscale and the extent to which organisms within the sputum environment would be expected to adapt to changes in the oxygen tension. To gain more insight into these aspects, we must consider the physical constraints of the lung. Figure 1 provides an overview of the respira-

tory airways starting from the trachea and branching downward into the smallest respiratory airways, the alveoli. The airway surface layer becomes dehydrated and viscous in CF patients. The ciliated epithelium is unable to clear the thickened mucus by moving it to larger airways, leading to obstructed airways and complete blockages. Early lung disease is observed initially in the bronchioles, alveolar sacs, and alveoli, as they are most easily blocked by mucus aggregation. We illustrate three possible deleterious scenarios: an entire airway can become blocked, although this is less common in CF (Fig. 1A); airway surface layers can thicken, resulting in restricted airflow (Fig. 1B); and, finally, a mucus plug can become dislodged and move into a larger airway (Fig. 1C). Expectorated sputum can have diverse airway sources. Expectoration clears the airways only temporarily, and exacerbation itself can cause larger volumes of sputum to be produced; patients with greater disease severity generally produce more sputum.

Ultimately, the electron accepters and the nutrients available in dynamic environments such as CF sputum dictate which microbial metabolisms will be possible. In turn, microbial depletion of oxygen and nutrients, as well as the generation and accumulation of metabolic products, can modify local chemistry and provide information on microbial activities. This predicts a dynamic sputum microenvironment with metabolically versatile microbial communities that adapt to or evolve with changing chemical parameters. In this study, we sought to characterize the CF sputum environment at the microscale through direct measurements of samples from different patients over extended time periods. Using modeling, we constrain how these measurements map to geometries of relevance within CF airways.

RESULTS

Apart from a thin oxic surface layer, all sputum samples are anoxic. As a first step toward constraining the *in vivo* environment, we used oxygen microsensors to profile freshly expectorated sputum (see Materials and Methods). A total of 48 different sputum samples from 22 different pediatric patients living with CF were profiled for oxygen, and all measurements were performed within 15 min of expectoration. This time period was the shortest allowed by sample processing constraints. Control experiments were performed to determine whether the time elapsed after expectoration affected the oxygen concentrations. Oxygen profiles measured in the same sputum sample at different starting positions and different time intervals, from 6 min to 4 h after collection, demonstrated similar patterns with very little variation over time in oxygen penetration depth (see Fig. S1 in the supplemental material). This likely reflects a steady state between oxygen diffusion into the sputum sample and consumption. As previously seen (14), we observed a characteristic oxygen profile using a Clark-type amperometric microelectrode (detection limit of 0.30 μM), consisting of a steep oxycline at the top of the air-sputum interface leading to an anoxic zone (0 μM O_2), for all samples. Effectively zero O_2 availability in the anoxic zone was confirmed by using an amperometric switchable trace oxygen (STOX) sensor (32), which can detect ultralow (as low as 2 nM) oxygen concentrations (Fig. 2A). Six samples were profiled with the STOX sensor, 3 of which were also profiled with the standard O_2 microelectrode. Since negligible O_2 levels were detected in all STOX electrode profiles, all subsequent profiles were profiled with the standard O_2 sensor only. Figure 2B displays the oxycline leading to anoxia for 5 of the smaller samples by volume ($<$1,000 mm^3), while Fig. 2C displays the oxycline and subsequent anoxic zone for 5 of the samples with larger volumes ($>$1,000 mm^3). The average volumetric fraction of all samples containing detectable oxygen was ~30% ($n = 20$).

Sputum redox profiles exhibit spatiotemporal variability. Having established that anoxia characterizes the main volume of all expectorated sputum samples, we measured the oxidation-reduction potential (ORP) by profiling 28 samples with a redox microelectrode in tandem with the oxygen sensor. As shown in Fig. 3, the ORP profiles could be separated into two groups: one comprising 17 samples with a positive redox potential range (16 mV to 355 mV), representing an oxidized, albeit anoxic, microenvironment (Fig. 3A), and another comprising 11 samples displaying a negative redox potential range ($-$300 mV to $-$107 mV), indicating a reducing microenvironment (Fig. 3B). Four patients profiled on multiple days showed different redox states at different times (see Table S1 in the supplemental material).

Reduced sputum samples show an accumulation of hydrogen sulfide. To identify a possible redox couple setting the potential of highly reduced samples, we added an amperometric hydrogen sulfide (H_2S) sensor (33), mindful that a low redox potential may be caused by the presence of reduced sulfur compounds. Twenty-three sputum samples from 17 patients were profiled simultaneously using one O_2, one redox, and one H_2S microsensor. Sixteen samples grouped into the more oxidized ORP class (ORP $>$ 0 mV), and H_2S was detected in 1 of those samples (Fig. 4A). Seven of the samples fell into the more reduced class (ORP $<$ 0 mV), and H_2S was detected in 5 of those samples (Fig. 4B). We also measured pH profiles of the sputum samples with detectable H_2S, in parallel to the H_2S profiles, revealing a pH range of 2.9 to 6.5 (see Table S2 in the supplemental material). Additionally, we profiled 4 samples without detectable H_2S with the pH sensor, finding 3 to be acidic and 1 basic (see Table S2). Intriguingly, 4 individuals presented sulfidogenic sputum on some occasions but not all.

All H_2S microprofiles were recalculated and displayed as total sulfide concentrations using the corresponding pH values ($\sum H_2S = [H_2S] + [HS^-] + [S^{2-}]$); here, we use the term "sulfide" to represent all of those species (33, 34). The pH values were stable during the course of profiling, even over several hours. The total sulfide concentration values likely represent conservative estimates because they reflect only what is in the aqueous phase; given that ferrous iron levels in sputum can be high (17), it is possible that in some of our samples the presence of poorly soluble mineral phases, such as FeS, may have lowered the amount of detectable sulfide. To determine the rate of sulfide accumulation, we measured sulfide concentration profiles over time. An example of temporal sulfide accumulation is shown in Fig. 5A. In 5 of the 6 sulfidic samples, we could measure sulfide accumulation, with 4 of those shown in Fig. 5B. Sulfide concentrations increased at an average rate of 0.30 $\pm$ 0.25 μM/min ($n = 5$). Sulfide depletion was not observed in these samples over the course of measurement. The sulfidic samples and nonsulfidic samples were profiled on the same time scale; while the O_2 profiles were stable regardless of whether sulfide was detected, the fact that sulfide could accumulate over time in some samples indicates that they were not in the steady state. Nevertheless, the 15-min gap between expectoration and measurement is small enough to ensure that we captured *in vivo* conditions in our initial profiles.

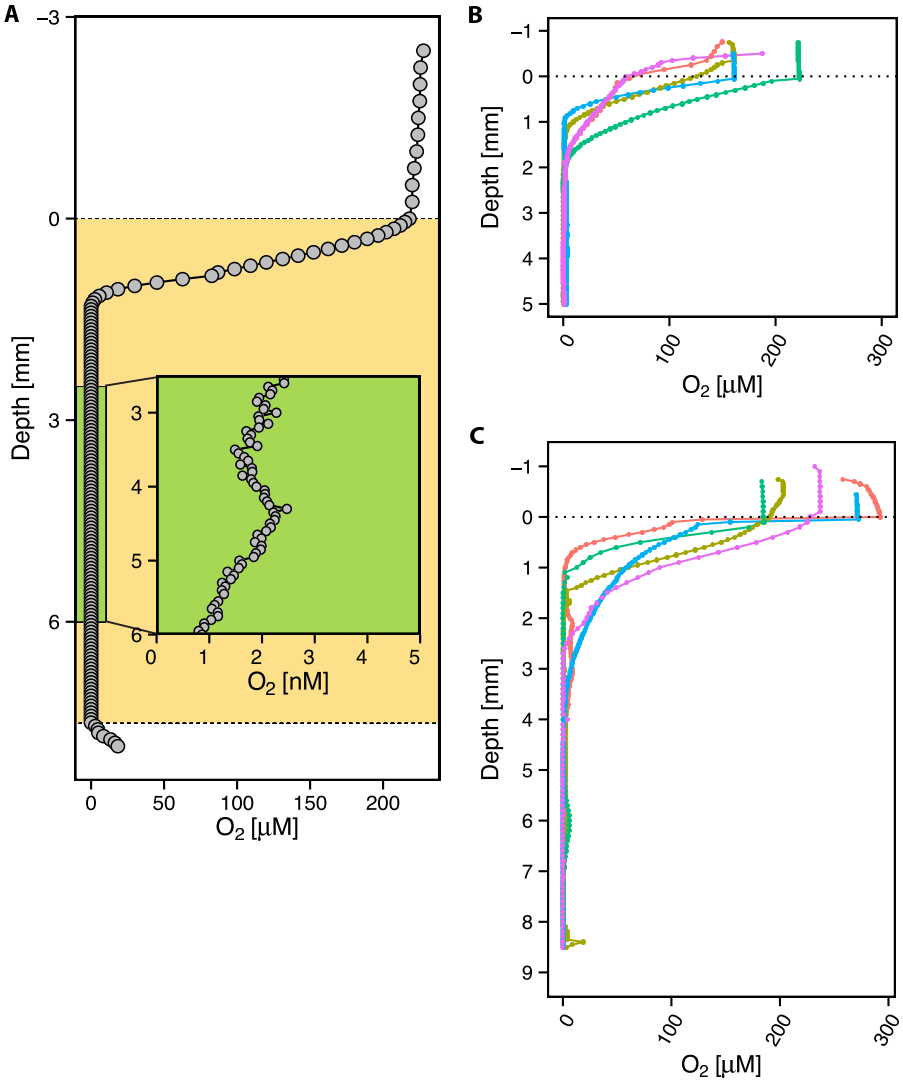

FIG 2 Representative oxygen microprofiles. (A) STOX microprofile, with the sputum sample marked in tan, representative of $n = 8$. The green rectangle shows an expanded view of a portion of the anoxic zone in the sputum sample. The detection limit is 2 nM. (B) Oxygen microelectrode profiles of 5-mm-deep expectorated sputum samples from 5 different patients, representative of $n = 12$. At the air-sputum interface, a steep oxycline begins and is followed by an anoxic zone that persists for the remaining portion of the sputum. (C) Oxygen microelectrode profiles of 8-mm-deep expectorated sputum samples from 5 different patients that were larger in volume, representative of $n = 27$. The same trend in profile occurs, with a steep oxycline followed by anoxia.

Inspired by the detection of N_2O in sputum from adults (14, 35) and in an effort to identify other redox couples responsible for the ORPs observed, we profiled 4 of our pediatric samples with O_2, H_2S, redox potential, and N_2O sensors. Only one sample had measurable N_2O, which accumulated in the anoxic zone but did so above the layer where sulfide was detected (see Fig. S2A in the supplemental material). The other 3 samples had no detectable H_2S or N_2O (see Fig. S2B).

Ion concentrations in sputum are variable, but high [NH_4^+] correlates with reduced samples. To gain insight into the variability in redox states and the potential for sulfide accumulation, we measured the inorganic ions present in sputum samples of sufficient volume to collect a filtrate. The average ion concentrations determined in randomized triplicate experiments in 21 sputum samples from 12 different patients profiled with the microelectrode were as follows: for Cl^-, 21.77 ± 14.92 (standard deviation [SD]) mM; for NO_3^-, 0.48 ± 0.57; for SO_4^{-2}, 0.32 ± 0.23; for Na^+, 26.63 ± 14.58; for NH_4^+, 4.92 ± 2.30; for K^+, 7.72 ± 4.78; for Mg^{+2}, 0.49 ± 0.32; and for Ca^{+2}, 1.32 ± 0.54.While large variations in ion concentrations were found, all reduced samples had higher concentrations of ammonium than the oxidized samples, with concentrations reaching as high as 10 mM (see Table S3 in the supplemental material). However, there was no appreciable difference in sputum sulfate concentrations between sulfidic samples (0.23 ± 0.15 [SD] mM sulfate) and nonsulfidic samples (0.33 ± 0.23 [SD] mM sulfate) (see Table S3), suggesting that sulfate reduction is unlikely to be the source of sputum sulfide. Taking patient 10, who had sulfidic and nonsulfidic samples, as an example, there was statistically no change in sulfate concentrations between samples, suggesting the absence of sulfate reduction.

Modeling predicts extensive sputum hypoxia and anoxia *in vivo*. While chemical measurements of freshly expectorated

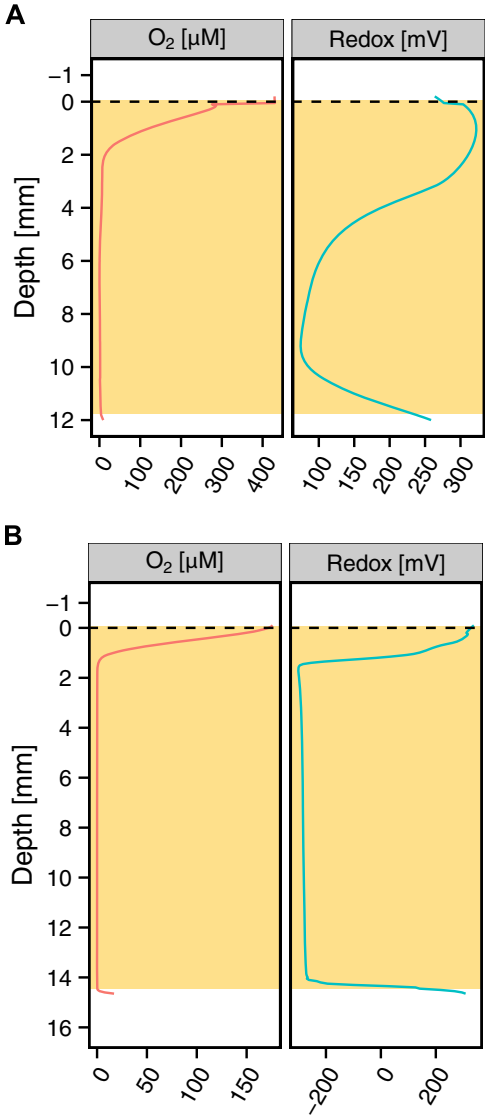

FIG 3 Representative examples of high and low sputum ORPs. The tan-shaded boxes indicate the extent of the sputum sample. (A) Of 23 of the redox-profiled samples, 11 displayed a positive redox potential (16 mV to 355 mV) indicative of an oxidizing microenvironment. (B) Of 23 of the profiled samples, 17 displayed a negative redox potential (−300 mV to −107 mV) indicative of a reducing microenvironment.

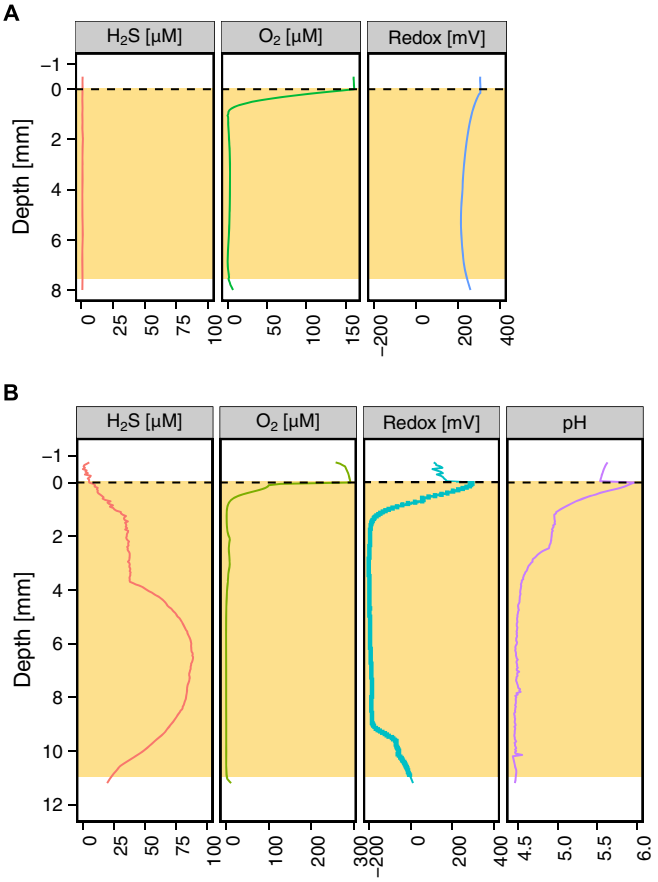

FIG 4 Representative examples of ORPs in tandem with H_2S detection. The tan-shaded boxes indicate the extent of the sputum sample. (A) A total of 14 of the 16 sputum samples that were highly oxidized samples (positive reduction potential) did not exhibit a presence of H_2S. (B) A total of 5 of the 7 sputum samples that were highly reduced (negative reduction potential) exhibited the presence of H_2S and were acidic.

sputum provide insight into the *in vivo* microenvironment, the geometry of our sampling vessels differs from that of the airways. Short of making microsensor measurements during bronchoscopies, which poses a variety of technical problems and potential health risks to the patient, we can constrain the *in vivo* relevance of our *ex vivo* microsensor profiles using models whose parameters are informed by our experimental measurements. Our model predicts sputum oxygen dynamics solely as a function of microbial growth and aerobic respiration. We assume inhaled air is the dominant source of oxygen for mucus. For simplicity, we assume microbial cell density to be homogenous and we neglect host oxygen consumption (e.g., by immune cells such as polymorphonuclear leukocytes [PMNs]) (36, 37), hemoglobin (Hb) in capillaries near the epithelium, and oxygen scavenging by reductive metabolites generated within sputum (e.g., sulfide). Creating a more complex model accounting for host oxygen consumption and reductive metabolite scavenging would lead to steeper oxyclines and lower bacterial densities to account for the oxygen concentrations. Accordingly, our model is conservative and likely overestimates oxygen content *in vivo*.

Within the airways, oxygen diffuses from the boundary layer at the air-mucus interface into the mucus. We can model mucus oxygen concentrations as a steady-state balance between oxygen diffusion and microbial respiration and as a function of mucus layer thickness, microbial density, and various physical and physiological constraints. This approach is an extension of a published model of oxygen diffusion into microbial colonies balanced by respiration (38). Briefly, the model is formalized as follows:

$$\frac{\partial [O_2]}{\partial t} = D_{O_2} \cdot \nabla^2 [O_2] - Q \cdot a \qquad (1)$$

where oxygen $[O_2]$ (mol $O_2 \cdot m^{-3}$) diffuses with diffusivity D_{O_2} ($m^2 \cdot s^{-1}$) depending on the local oxygen concentration gradient and is consumed at rate Q (mol $O_2 \cdot s^{-1} \cdot g$ cells^{-1}) by a respiring

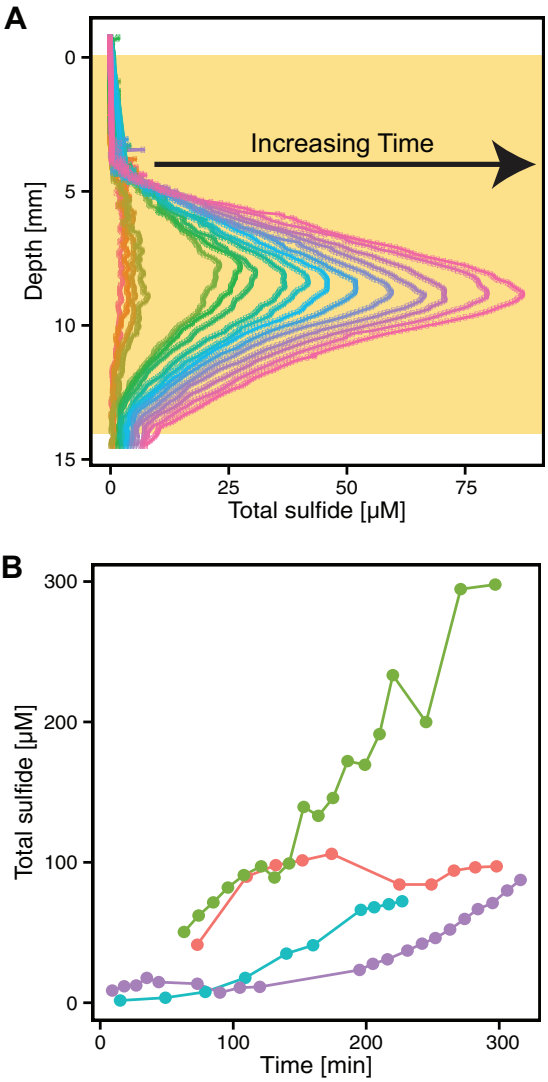

FIG 5 Sulfide can build up rapidly in sputum. (A) Dynamics of total sulfide production over time in one sputum sample incubated for a total of 240 min. Time increases from left to right (orange to pink). This is the same sample represented by the purple line in panel B. The tan box indicates the depth of the sputum sample. (B) Increases in sulfide levels over time in sputum samples incubated at 37°C for 4 different patients. Each color represents a different sputum sample profiled over time. Each time point represents the maximum sulfide concentration for a specific profile. Not all of the maxima were recorded at the same depth in the samples. For the sample represented by the red line, the average maximum sulfide depth was within the range of 6.85 to 7.40 mm; for the green sample, 9.85 to 13.30 mm; for the blue sample, 15.60 to 18.30 mm; and for the purple sample, 8.15 to 11.25 mm. Five of the sulfidic samples were profiled over a period of up to 300 min and demonstrated a significant increase in the sulfide level.

microbial community with density a (g cells $\cdot$ m^{-3}). Assuming O_2 to be the limiting nutrient in the system, the oxygen consumption rate Q can be expressed in terms of a Monod-type growth rate saturation model and a maintenance term:

$$Q = \frac{\mu}{Y_{O_2}} + P_{O_2} = \frac{\mu_{max}}{Y_{O_2}} \cdot \frac{[O_2]}{k_{O_2} + [O_2]} + P_{O_2} \qquad (2)$$

with a maximum specific growth rate μ max (s^{-1}), yield coefficient Y_{O_2} (g cells $\cdot$ mol O_2^{-1}), half-saturation constant k_{O_2} (mol $O_2 \cdot m^{-3}$), and the maintenance oxygen requirement P_{O_2} (mol $O_2 \cdot s^{-1} \cdot$ g $cells^{-1}$).

At the steady state $\left(\frac{\partial[O_2]}{\partial t} = 0\right)$, diffusion and respiration are balanced and describe a stable oxygen profile whose shape depends on the above-mentioned parameters as well as on constraints imposed by geometry-specific boundary conditions (see Materials and Methods for details).

Three relevant geometries to consider in the context of CF lung mucus aggregation are outlined in Fig. 1 (scenarios A, B, and C). By keeping the physical parameters (oxygen diffusivity, mucus thickness, etc.) and the physiological parameters (maximal growth rate, oxygen half-saturation, etc.—see Materials and Methods for details) constant but adjusting bacterial densities at realistic values for CF mucus (39), we explored how the shape of mucus in these different contexts might impact expected oxygen gradients. Despite the limited (500-μm) depth assumed for these calculations, the model predicts a steep oxycline leading to extensive anoxic zones at higher cell densities (Fig. 6), regardless of geometry. For comparison, Table 1 lists the maximal depths of oxygen penetration below which all mucus is anoxic for the two geometric extremes (dislodged spherical aggregates and single airway plugs) over a range of cell densities. By fitting 32 expectorated sputum oxygen microsensor profiles with our spherical mucus aggregate model, we infer average cell densities of 8.3×10^7 cell/ml for these sputum samples (see Table S4 in the supplemental material), which is in line with direct bacterial counts from other studies (39). Such fitting is justified because sputum itself is quite hydrated and surrounded by saliva, so the limiting diffusivity is always that of water. As indicated in Table 1, this suggested that, on average, at these densities, anoxic zones would be expected in clogged airways with mucus layer thickness greater than 1 mm.

The shape and thickness of the oxycline are also affected by all other physical and physiological parameters (see Materials and Methods and Table 2). Unlike cell density, however, most other physical and physiological parameters are unlikely to change by orders of magnitude. This reduces their potential effects on oxycline scaling, with oxygen diffusivity likely the second most impactful variable parameter. For comparison to Fig. 6, we illustrate the potential effect of variable oxygen diffusivities with 3 different literature estimates (for water, biofilm, and rat colon mucus) (see Fig. S3 in the supplemental material). We used the intermediate biofilm diffusivity value for all other modeling results.

Considering mucus restrictions in the lung to begin by a thickening of the normal airway surface layer, we modeled the two-dimensional (2D) distribution of oxygen in bronchioles to illustrate the spatial distribution. As for the 1D models shown in Fig. 6, we adjusted the bacterial density from 10^7 cells/ml to 10^{10} cells/ml; in addition, for the 2D models, we adjusted the mucus layer thickness from 50 to 400 μm based on reported values (40–43). Figure 7A reveals that airways with a 50-μm-thick layer of mucus would be expected to never become anoxic for the cell densities used in the model. In mucus layers that are 250 μm thick, anoxic conditions would be attainable only with very dense microbial populations (~10^9 cells/ml). In 400-μm-thick layers, however, anoxia could be reached at the epithelial cell boundary with population densities as low as 10^8 cells/ml. A corollary to the oxygen distributions modeled in Fig. 7A is that oxygen-dependent respiratory growth rates would range from low to zero in many cases

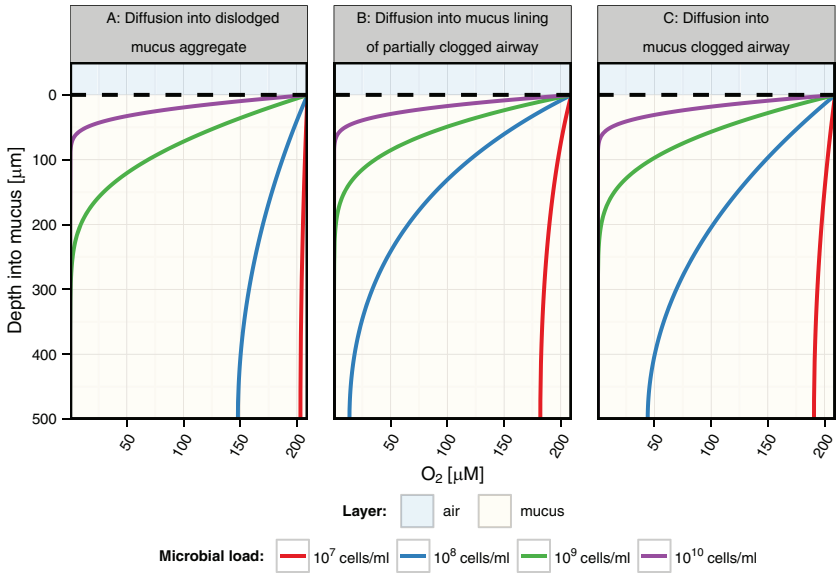

FIG 6 Comparison of levels of oxygen diffusion into mucus based on different respiratory airway geometry constraints and bacterial densities. Data represent oxygen diffusion into different respiratory airways clogged with mucus at various bacterial densities. The described scenarios correspond to the diagram in Fig. 1 with a modeled mucus thickness (x) of 500 μm and an airway diameter of 1.5 mm for scenario B (model scenarios A and C are not affected by the airway diameter). The upper blue shaded area indicates air, and the tan lower layer indicates mucus.

(Fig. 7B). Again, we hasten to note that this simple model neglects oxygen consumption by the host as well as abiotic oxidation by reduced metabolites; thus, its predictions with respect to oxygen abundance are conservative. Accordingly, it is probable that hypoxia and anoxia dynamically occur *in vivo* and would likely dominate the microenvironments in larger regions of the airways even at relatively low cell densities (e.g., 10^7 cells/ml). Collectively, these results reinforce the importance of considering mechanisms of adaptation to variable oxygen concentrations within the CF lung.

Clinical data. Of the 48 samples profiled, 32 were also cultured for dominant CF pathogens by the Children's Hospital Los Angeles (CHLA) clinical microbiology laboratory. As shown in Table S1 in the supplemental material, 13 samples harbored *P. aeruginosa*, 12 contained *Staphylococcus aureus*, 5 were positive for both *P. aeruginosa* and *S. aureus*, and 2 had neither pathogen.

TABLE 1 Modeled oxygen penetration depths (i.e., oxycline thickness) for mucus-clogged airways and dislodged mucus aggregates with various bacterial densities[a]

Density (cells/ml)	Diffusion into dislodged mucus aggregate	Diffusion into mucus-clogged airway
1.00E+05	39 mm	28 mm
8.10E+05	14 mm	9.7 mm
1.00E+06	12 mm	8.8 mm
1.00E+07	3.9 mm	2.8 mm
8.30E+07	**1.3 mm**	**960 μm**
1.00E+08	1.2 mm	880 μm
1.00E+09	390 μm	280 μm
1.30E+09	340 μm	240 μm
1.00E+10	120 μm	88 μm
1.00E+11	39 μm	28 μm
1.00E+12	12 μm	8.8 μm

[a] The data in the row in boldface type closely match the average profiles from our experimental data.

The presence of a specific organism did not significantly correlate with the reduction potential state, pH, or presence of sulfide (see Table S5 in the supplemental material). However, of the clinical parameters reviewed (including age, sex, race, diagnosis of pancreatic insufficiency, cystic fibrosis-related diabetes, gastroesophageal diseases, CF liver disease, or allergic bronchopulmonary *Aspergillus* infection, hemoglobin A1c [HbA1c] levels, IgE levels, blood glucose levels, sputum iron levels, visit reason [inpatient or outpatient], height, weight, body mass index [BMI], intravenous [i.v.] antibiotic status, supplementary-oxygen status, pulmonary exacerbation, antibiotic and other medication, cultured microbes, and spirometry results; see Tables S1 and S5) for the 23 samples profiled for sulfide, the presence of sulfide was positively correlated with reduced reduction potential ($P < 0.001$), increased IgE values, lack of supplemental oxygen, a decreased likelihood of the subject being an inpatient, and larger sputum samples ($P < 0.05$) (see Table S5). Although we do not have enough patient samples to support a statistically significant correlation at present, we note

TABLE 2 Modeling constants

Constant	Value	Unit(s)
Oxygen diffusion coefficient in water (86)	26.8	10^{-6} cm^2·s^{-1}
Oxygen diffusion coefficient in biofilm (86)	15.3	10^{-6} cm^2·s^{-1}
Oxygen diffusion coefficient in rat colon mucus (87)	2.4	10^{-6} cm^2·s^{-1}
Oxygen half-saturation constant (38)	0.0124	Mol O_2 m^{-3}
Maximal growth rate (38)	0.00023	s^{-1}
Growth yield (88)	20.32	g·cell/mol O_2
Maintenance coefficient for O_2 (38)	1.22	10^{-7} mol O_2 g cell^{-1} s^{-1}
Cell density (39)	9.1	Log (cells / ml)
Cell weight (38)	2.14	10^{-12} g/cell
Oxygen at air-mucus boundary (79)	209.3	μM

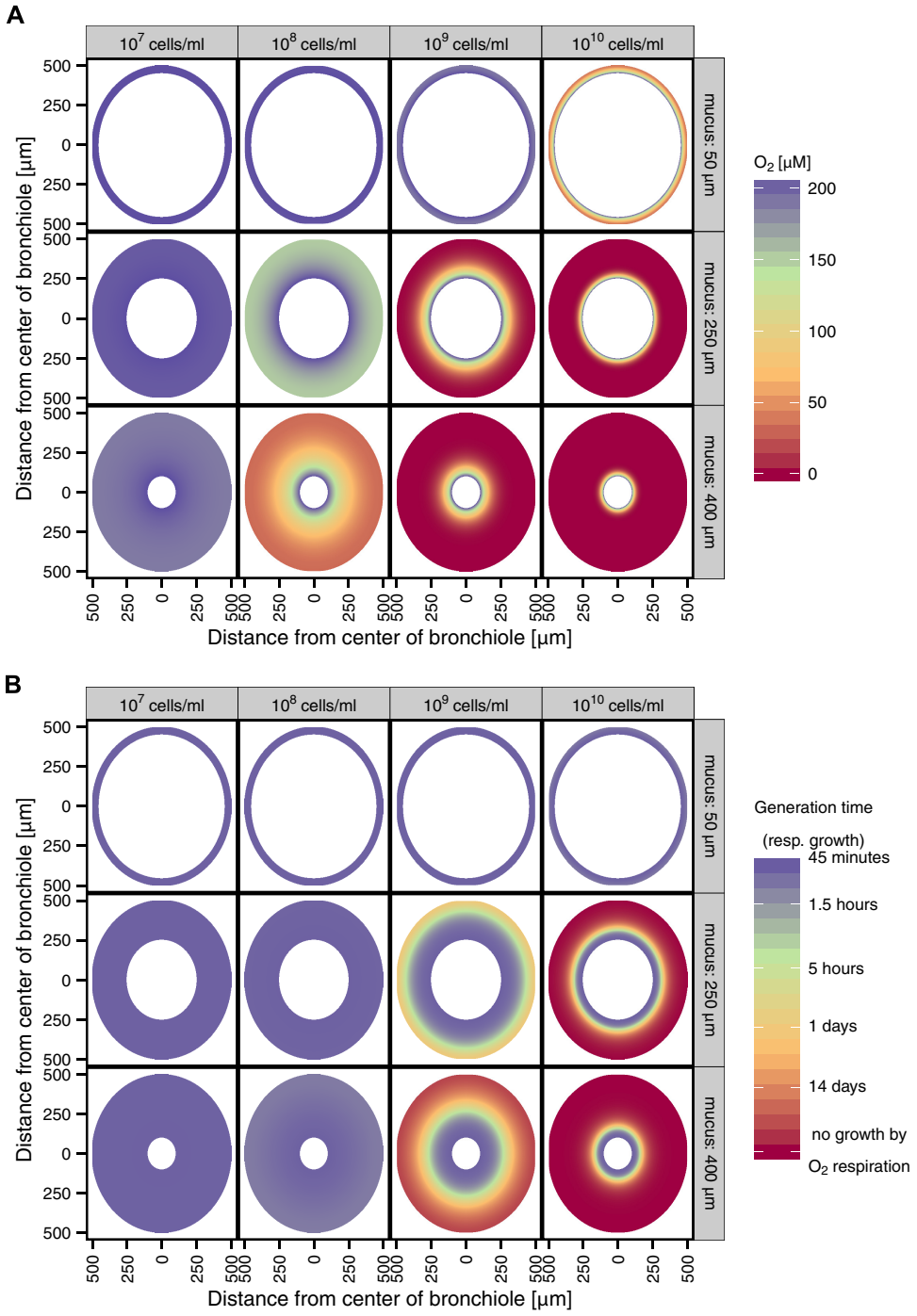

FIG 7 Predicted oxygen concentrations and generation times due to aerobic respiration in bronchioles clogged with mucus. (A) Differential oxygen concentrations affecting the thickness of the mucus and the bacterial density. (B) A two-dimensional visualization of the bronchiole with variation in the mucus thickness and bacterial density and the resulting predicted generation time of the pathogens in the mucus during growth only via aerobic respiration (resp.). This accounts only for aerobic respiration and neglects other catabolic pathways.

that reduced samples and the presence of sulfide were found in sputum from patients with mild to moderate lung function impairment but not in those who were severely impaired (see Table S1).

For the 30 samples profiled for reduction potential, an oxidized environment significantly correlates with cystic fibrosis-related diabetes (CFRD) ($P < 0.01$), a lack of sulfide ($P < 0.01$), and the presence of methicillin-sensitive *S. aureus* ($P < 0.05$) (see Table S5 in the supplemental material).

DISCUSSION

In this study, we measured sputum inorganic chemistry in a large pediatric cohort of children living with CF from Children's Hospital Los Angeles (CHLA). By using a suite of microelectrodes and

making multiple measurements of sputum from individual patients, we were able to determine the extent of chemical variability both within and between patients. In all samples, oxygen was depleted rapidly within a narrow oxycline, rendering the majority of the sputum anoxic. Moreover, the anoxic regions presented a strikingly large range of oxidation-reduction potentials that were both spatially and temporally variable; the lowest redox potentials measured (−300 mV) appear to have been caused by production and accumulation of sulfide. Even at different spatial scales within the lung, anoxia would be expected to constitute a significant fraction of the *in vivo* sputum environment. These results are directly relevant with respect to informing laboratory studies for elucidation of mechanisms of microbial adaptation and survival within CF lung infections.

Oxygen availability is one of the most critical inorganic parameters that determine microbial activity (44). Ironically, despite the fact that infections take hold in the lung, the site of oxygen intake to the body, the results of our studies demonstrate that the mucus microenvironment rapidly becomes anoxic and even reduced in the presence of sulfide. Two other studies have previously shown that the sputum microenvironment contains hypoxic and anoxic zones (12, 14). Yet one may question whether the oxygen sensors used in those studies were sufficiently sensitive to detect the low levels of oxygen that can sustain microbial growth. This concern is partially allayed by our profiles utilizing the ultrasensitive STOX system, which had a detection limit of 2 nM. While the minimum oxygen requirement for aerobic respiration by most CF pathogens is unknown, *Escherichia coli* can respire down to levels of ≤3 nM (45). While it is reasonable to expect that appreciable hypoxic zones occur *in vivo*, our modeling studies strongly suggest that the extent of hypoxia versus anoxia depends on the local geometry and microbial density. It is therefore most probable that CF sputum is spatially heterogeneous, spanning oxygen-replete layers located just at and below the air-sputum interface, hypoxic zones within a thin oxycline, and entirely anoxic microenvironments that may dominate the majority of the sputum below the oxycline. We underscore that our model is conservative, ignoring host oxygen consumption and reductive metabolite (e.g., sulfide) scavenging. A previous study demonstrated that oxygen consumption by host immune cells, PMNs, is likely the major oxygen sink within sputum, suggesting that even steeper oxyclines than those predicted by our model and lower bacterial densities are required to account for the oxygen concentrations (36). Growth using oxygen becomes diffusion limited based on our modeling and experimental measurements, suggesting that microbes need to shift to anaerobic metabolisms or enter a no-growth survival state.

While this conclusion is not surprising given the extensive documentation of oxygen limitation in other stratified microbial habitats (46–50), the large range of reduction potentials measured in different anoxic sputum samples was unexpected. Moreover, that these different redox states can exist not only between different patients but also at different times within the same patient highlights the dynamic character of the sputum microenvironment—something that is not typically considered. Intriguingly, in most cases (20 of 23), the presence or absence of sulfide correlated with highly reduced reduction potentials. Because many oxidized and reduced sulfur redox pairs have low redox potentials (51), it seems likely that reduced sulfur species were controlling the reduction potentials measured in these samples and that their pH levels were uniformly low. This suggests that monitoring breath sulfide may afford a means to assess the redox state within a patient's lungs; detecting hydrogen sulfide in the breath is not unprecedented (52–54). That total sulfide can accumulate in some samples at a rate of 0.30 μM/min demonstrates the considerable potential for sulfide production *in vivo*; however, sulfide would not be expected to accumulate *in vivo* to the levels measured unless it were generated in mucus plugs greater than 1 mm in thickness when the microbial load is ~8×10^7 cells/ml. It is noteworthy that we did not detect sulfide in every reduced sample, suggesting that other metabolites with low redox potentials must contribute to setting the redox state in some cases or that the sulfide is not available for detection with the sensors. In the three cases with low reduction potentials and yet undetectable sulfide, organic metabolites, such as phenazines—which are known to be generated in sputum and have a broad range of reduction potentials (16, 55)—might instead help set the redox potential. Regardless, samples with reduced reduction potentials had a higher concentration of ammonium, potentially indicating a fermentative source of ammonium (31); even lower potentials could correspond to acetogenesis (56).

We do not yet know whether sulfide generated *in vivo* originates from a microbial or human source. Of relevance to the former, our major ion analysis for 6 patients and 6 samples indicates that sulfate is present at 0.23 ± 0.15 (SD) mM. Though sulfate-respiring bacteria (SRBs) could in principle be a source of sputum sulfide (possibly entering from the gut [57]), neither we nor others have found evidence for their presence (31, 58–60). Sulfide could also be a byproduct of amino acid degradation mediated by the microbial community (61–64). It is perhaps more likely that sulfide is being generated from arginine, cysteine, and homocysteine as a defense mechanism against oxidative stress, as has been demonstrated to occur for *S. aureus* and *P. aeruginosa* in laboratory experiments (65). Disentangling these possibilities awaits future research.

Taking our environmental measurements into consideration, we can speculate on how particular chemical variables might impact the metabolic strategies of members of the CF microbial community. Extensive hypoxia and anoxia would favor organisms adept at generating energy in the absence of oxygen. Consistent with this prediction, the major CF pathogens, including *P. aeruginosa*, *S. aureus*, *Burkholderia cepacia*, *Stenotrophomonas maltophilia*, *Haemophilus influenzae*, *Klebsiella pneumoniae*, *Escherichia coli*, *Achromobacter xylosoxidans*, and *Aspergillus fumigatus*, are all capable of aerobic and anaerobic metabolisms. Table 3 lists representative anaerobic metabolisms (both respiratory and fermentative) that previous studies have identified as being relevant in the CF lung, ranked in order from greatest- to least-energy-yielding capacity under standard conditions using lactate as a carbon source (15, 66, 67). Assuming the presence of chemical species that would dominate at neutral pH, we can predict whether these metabolisms would be thermodynamically favored or inhibited by lowering pH. The acidic pH measured in many of our samples would favor aerobic respiration, denitrification, sulfate reduction, fumarate reduction, and acetoclastic methanogenesis. In contrast, basic pH would favor acetogenesis. Altering the pH would not be expected to affect hydrogenotrophic methanogenesis. We note that these predictions do not take into consideration the actual *in*

TABLE 3 Net reactions of metabolisms likely to be important in sputum with sensitivity to pH and metabolic pathway modeling and pH influence[a]

Metabolic pathway	Reaction	$\Delta G^{o'}$ (kJ/mol lactate)	$\Delta E^{o'}$ (mV)	ΔG (pH = 4) (kJ/mol lactate)	ΔE (pH = 4) (mV)	Relative effect of low pH	Reaction context in sputum
Aerobic respiration	$C_3H_5O_3^- + 3O_2 + H^+ \rightarrow 3CO_2 + 3H_2O$	−1337	1160	−1354	1170	1.3% more energetic	22
Denitrification	$5C_3H_5O_3^- + 12NO_3^- + 17H^+ \rightarrow 15CO_2 + 6N_2 + 21H_2O$	−1262	1090	−1320	1140	4.6% more energetic	14, 31, 35
Fumarate reduction	$6\,C_4H_2O_4^{2-} + C_3H_5O_3^- + 3H_2O + H^+ \rightarrow 6\,C_4H_4O_4^{2-} + 3CO_2$	−432	370	−449	390	4% more energetic	31
Sulfate reduction	$3SO_4^{-2} + 2\,C_3H_5O_3 + 8\,H^+ \rightarrow 3H_2S + 6CO_2 + 7H_2O$	−139	120	−207	180	47% more energetic	31
Acetoclastic methanogenesis	$C_2H_3O_2^- + H^+ \rightarrow CH_4 + CO_2$	−37[b]	48	−54[b]	70	31% more energetic	90
Hydrogenotrophic methanogenesis	$CO_2 + 4\,H_2 \rightarrow CH_4 + 2\,H_2O$	−33[b]	170	−33[b]	170	No effect	90
Acetogenesis	$2CO_2 + 4\,H_2 \rightarrow C_2H_3O_2^- + H^+ + 2H_2O$	−24[b]	123	−19[b]	101	20% less energetic	91

[a] Standard reduction potential differences ($\Delta E^{o'}$) and standard Gibbs free energies ($\Delta G^{o'}$) were derived from reduction/oxidation half-reactions (51, 89) and calculated at standard temperature (25°C) and pressure (1 atm) at pH 7, indicated by prime notation.
[b] ΔG values for the reactions are per mole H_2 and per mole acetate.

vivo concentrations of all the relevant chemical species that would be necessary to estimate the true thermodynamic favorability of any particular metabolism and also do not consider kinetic effects. However, in general, it is reasonable to conclude that the low-pH regimens observed in many of our samples are consistent with the thermodynamic progression of several important types of anaerobic metabolisms.

Beyond impacting energy generation pathways, the chemical parameters we have measured would be expected to affect the microbial community in other ways. For example, it is known that for *S. aureus*—one of the dominant culturable organisms in our patients—low or high pH inhibits growth and/or biofilm formation (55–57). At low pH, *S. aureus* upregulates virulence genes, including several that are also upregulated in response to antibiotics (68, 92); consistent with this response, *S. aureus* is more resistant to aminoglycoside drugs at low pH (69). Similar pH effects on virulence gene expression and antibiotic resistance have been found for other pathogens as well (70).

How might sulfide affect microbial or host cell activities? One means could be to block particular enzymatic activities. Intriguingly, in the one sample where we measured N_2O levels, the reduction potential was highly positive where N_2O was present, as expected for an anoxic zone dominated by denitrification (51), and yet the potential decreased in the portion of the sample where sulfide was detected. N_2O is primarily an intermediate in nitrification or denitrification processes, requiring oxygen or nitrate, respectively, which might explain its occurrence in the upper portion of the sputum. Because sulfide can inhibit nitrous oxide reductase, which catalyzes the conversion of N_2O to N_2, the presence of sulfide could explain the accumulation of N_2O in this sample. The consequence of such an inhibitory effect would be metabolic stratification to different sputum zones. It is also possible that sulfide generation would alter the bioavailability of ferrous iron, which is typically found in concentrations of 10 mM to 100 mM in sputum (17), through precipitating ferrous sulfide minerals (51). Finally, sulfide would be expected to impact microbial and host cells in its capacity as a gasotransmitter (71).

Might sulfide be a viable disease biomarker and potential diagnostic tool for patients living with CF? Sulfide has been used as a disease biomarker and is considered a potential diagnostic tool in other clinical settings. As a gasotransmitter, sulfide participates in regulating the inflammatory response (72) by being a proinflammatory signal or an anti-inflammatory signal, depending on the situation (73). Although the role of sulfide in the inflammatory response is complex and not entirely understood, it has been shown to be a critical mediator in chronic obstructive pulmonary disease (COPD). Levels of H_2S were increased as COPD progressed and became more severe (74). Consistent with this trend, a previous study of CF patients measured carbonyl sulfide, dimethylsulfide, and carbon disulfide concentrations in exhaled breath; higher concentrations of carbonyl sulfide correlated with poorer lung function (75). However, sulfide levels were not measured in this study and the source of the exhaled sulfur compounds was unclear. Interestingly, in asthma and pulmonary fibrosis, sulfide has been found to have a countercorrelation, with healthier patients having higher levels of sulfide in serum and breath (76–78). More research is needed to determine whether any statistically significant correlation exists between breath sulfide and lung function in CF, although we did observe a statistically significant negative correlation between sulfide presence and inpatient status, suggesting that sulfide could be a biomarker of good health in CF. The observed negative correlations between sulfide abundance and patients needing supplemental oxygen or patients being hospitalized also support this idea.

In summary, this study has revealed significant spatial and temporal heterogeneity in major inorganic parameters that characterize CF sputum both within and between patients. These chemical dynamics likely reflect physiological adaptations with a metabolically versatile microbial community that

are responsible, in part, for the generation of compounds that impact the redox state of the sputum environment. Heightened awareness of the extent of sputum anoxia, low pH, and the potential for a fluctuating redox state can inform future research into the survival mechanisms that pathogens utilize under these conditions. From a point-of-care standpoint, it is worth considering whether different chemical fingerprints from sputum might improve the ability of clinicians to diagnose the extent of lung disease. Determining whether particular metabolic fingerprints correlate with disease progression and, if so, which treatments would be most effective under these conditions should be a priority for future work.

MATERIALS AND METHODS

Collection technique. Cystic fibrosis patients from Children's Hospital Los Angeles were recruited for this study, with the criteria of the patients being at least 4 years old and having a positive CF diagnosis and the ability to expectorate sputum. Patient consent and assent were obtained in accordance with Institutional Review Board (IRB) no. CCI-13000211. Sputum samples were collected from patients upon expectoration.

Chart review. A review of the patients' medical records from January 2012 to November 2014 was performed to obtain a variety of clinical parameters, including age, gender, reason for hospital visit, height, weight, BMI, and pulmonary lung function (see Table S1 in the supplemental material).

Microelectrode profiling. After collection, sputum samples were immediately transferred to 3-ml cylindrical cavities molded into 20 ml of agar in a truncated 50-ml Falcon tube. The tubes were placed in a heating block to maintain a constant temperature of 37°C prior to and throughout any measurements.

Six different microsensors were used throughout this study: an O_2 microsensor with a tip diameter of 25 μm, a STOX sensor with a tip diameter of 50 μm, an N_2O microsensor with a tip diameter of 25 μm, an H_2S microsensor with a tip diameter of 50 μm, a pH microsensor with a tip diameter of 25 μm, and a redox electrode with a tip diameter of 50 μm in tandem with an Ag/AgCl needle reference electrode.

The O_2, N_2O, and H_2S microsensors are all amperometric sensors and were connected to picoampere amplifiers in a multimeter (Unisense, Denmark). The redox and pH electrodes were both connected to high-impedance millivoltmeter inputs in the same multimeter.

The O_2 is a Clark-type amperometric electrode with a detection limit of 0.30 μM. The O_2 sensor responds linearly to changes in oxygen concentration; thus, a two-point calibration was performed by immersing the sensor tip in an oxygen-free solution made of sodium hydroxide and sodium ascorbate (both at a final concentration of 0.1 M) to obtain the zero-oxygen reading and in a 100%-air-saturated 0.72% salt solution, which corresponds to 209.3 μM oxygen at the given temperature and salinity level (79). The switchable trace oxygen (STOX) sensor is a specific measuring unit for detecting trace amounts of oxygen with a reported detection limit of 2 nM. The design of the STOX sensor was also based on an amperometric oxygen sensor but was modified by adding a second cathode, which can be switched on and off via a controller unit that is connected between the sensor and the multimeter. This second cathode, or front guard, consumes any traces of oxygen that might enter the electrode, thus enabling reliable measurements of ultralow oxygen concentrations (80).

The H_2S sensor was similarly linearly calibrated, with the zero point being taken in a 0.72% salt solution and the second point by immersing the sensor in a 100 μM H_2S solution prepared in an alkaline buffer solution that was kept anoxic by adding a reductant [Ti(III)Cl]. The sensor has a detection limit of 0.30 μM (33).

The N_2O sensor is also a Clark-type electrode, with a detection limit of 0.50 μM. The sensor is equipped with an oxygen front guard to prevent interference with the N_2O measurement (81). The N_2O sensor was linearly calibrated with the zero-point measurement taken in an N_2O-free 0.72% salt solution; subsequently, a specified volume of N_2O-saturated Millipore water was added to reach a concentration of 66 μM N_2O for a second calibration point.

The pH electrode was calibrated with buffers of pH 4, 7, and 10 (82). The electrode has a detection limit of 0.1 pH unit. The redox electrode was used together with an Ag/AgCl reference electrode to establish the redox potential, and the values are given relative to the standard hydrogen electrode (SHE) and were determined by measuring the offset of the reference electrode in saturated quinhydrone buffer solutions (pH 4 and pH 7) with known redox potentials. The electrode has a detection limit of 0.10 mV (83). All calibrations were done at the experimental temperature of 37°C and at 0.72% salinity. Microsensors were mounted on a motorized micromanipulator in a custom-made probe holder, allowing three sensors to be used simultaneously. The reference electrode for redox and pH measurements was mounted separately in a free-standing ring stand and remained in one place in the sample throughout the measurements that was not controlled by the motorized micromanipulator. All microsensors and related equipment were purchased from Unisense A/S, Århus, Denmark.

In sets of three, sensors were positioned exactly at the air-sputum interface ("depth zero") by visual inspection using a Leica MZ 9.5 stereomicroscope. Automatic profiling and data acquisition were controlled using SensorTrace Pro 3.1.3 software. Vertical profiles were measured in intervals of 50 or 150 μm through the sputum samples. At each depth, the measuring time was set at 3 s with 2 s between measuring points for all sensors. The time interval between adjacent profiles in the same sample was 60 s. The profiles extended into the agar and began at least 250 μm above the surface of the sputum to determine the boundaries of the sputum sample easily. All samples were profiled, and the sensor was never positioned at a specific spot to log the concentration over time; rather, for data logging of maxima over time, multiple profiles were determined and the maximum concentration from each individual profile was plotted as a function of time since expectoration.

After profile completion, samples were removed from the agar plugs, added to a sterile tube, flash frozen in liquid nitrogen, and stored at −80°C. Time until freezing varied depending on the time course of the profiles recorded and ranged from 30 min to 25 h.

Ion chromatography. Anion and cation concentrations in the sputum samples were determined using a Dionex ICS-2000 ion chromatography system with AS-19 and CS-12A columns, allowing simultaneous measurement of anions and cations during one sample run. Sputum samples were thawed and centrifuged at 5,000 rpm for 10 min. The supernatant was filtered on a 0.20-μm-pore-size filter at 10,000 rpm for 20 min. Filtered sputum supernatants were diluted in a 1:50 ratio with Millipore water before analysis.

Clinical correlations. Correlations were calculated in R using Spearman rank analysis. Statistical significance was evaluated using the *P* value of the test statistic, with common thresholds used to group significance levels (0.01 = highly significant; 0.05 = significant).

Modeling. For modeling oxygen concentrations in CF mucus, we considered three different key geometries as outlined in Fig. 1. The simplest case (Fig. 1A) considers a completely blocked airway, which is approximated as a column of mucus that allows diffusional gradients in one dimension (distance x along a line into the mucus column). In this scenario, the Laplacian simplifies to $\nabla^2 = \frac{\partial^2}{\partial x^2}$ and equation 1 at the steady state becomes the following:

$$D_{O_2} \cdot \frac{\partial^2[O_2]}{\partial x^2} = Q \cdot a = 0 \quad (3a)$$

We used the following assumptions to inform the boundary conditions for equation 3a, taking a conservative approach that places an upper, maximal bound on the oxygen concentrations throughout the modeled mucus. First, oxygen diffusion from the gaseous into the aqueous phase at the air-mucus interface was assumed to be much faster than diffusion

deeper into the mucus, which implies a constant oxygen maximum $O_{2_{max}}$ at $x = 0$. Second, no oxygen gradient was assumed to develop across the boundary at the maximum distance from the air-mucus interface x_{max} (e.g., across the mucus-epithelial cell boundary). This equates to the following:

$$[O_2](x = 0) = O_{2max}$$

$$\left.\frac{\partial [O_2]}{\partial x}\right|_{x=x_{max}} = 0$$

The second scenario (Fig. 1B) describes an airway that is covered with a mucus layer of variable thickness. Assuming oxygen in air to be subject to very subtle gradients only when flowing through bronchioles, the bronchioles can be idealized as long radially symmetric cylinders with a homogenous mucus layer lining the inner wall of the cylinder and oxygen diffusing outward into the mucus. This can be described by expressing equation 1 in cylindrical coordinates with radius r, angular coordinate θ, and height z, in which case the Laplacian equation is $\nabla^2 = \frac{\partial^2}{\partial r^2} + \frac{1}{r}\frac{\partial}{\partial r} + \frac{1}{r^2}\frac{\partial^2}{\partial \theta^2} + \frac{\partial^2}{\partial z^2}$. Approximating the bronchioles as an infinite hollow cylinder without variation in $[O_2]$ along its length $\left(\frac{\partial [O_2]}{\partial z} = 0\right)$ and with radial symmetry $\left(\frac{\partial [O_2]}{\partial \theta} = 0\right)$, equation 1 at the steady state becomes the following:

$$D_{O_2} \cdot \left(\frac{\partial^2}{\partial r^2} + \frac{1}{r}\frac{\partial}{\partial r}\right)[O_2] - Q \cdot a = 0 \quad (3b)$$

Here, the same assumptions previously considered for the first scenario translate to an oxygen maximum at the inner mucus boundary (air-mucus interface) at distance r_1 from the center of the bronchiole and a reflecting boundary at outer radius r_2 (with $r_2 = 1/2$ the bronchiole diameter and mucus thickness $r_2 - r_1$):

$$[O_2](r = r_1) = O_{2max}$$

$$\left.\frac{\partial [O_2]}{\partial r}\right|_{r=r_2} = 0$$

The third scenario we considered (Fig. 1C) is a dislodged mucus plug that has a roughly spherical geometry, with oxygen diffusing inward from the surface at radius r_{plug} into the center of the plug ($r = 0$). This can be described by expressing equation 1 in spherical coordinates with radius r, polar angle θ, and azimuthal angle ϕ, in which case the Laplacian equation is $\nabla^2 = \frac{\partial^2}{\partial r^2} + \frac{2}{r}\frac{\partial}{\partial r} + \frac{1}{r^2}\frac{\partial^2}{\partial \theta^2} + \frac{1}{r^2}\frac{\cos\theta}{\sin\theta}\frac{\partial}{\partial \theta} + \frac{1}{r^2 \sin^2\theta}\frac{\partial^2}{\partial \phi^2}$. Assuming radial and azimuthal symmetry in the oxygen concentrations $\left(\frac{\partial [O_2]}{\partial \theta} = 0;\ \frac{\partial [O_2]}{\partial \phi} = 0\right)$, equation 1 at the steady state becomes the following:

$$D_{O_2} \cdot \left(\frac{\partial^2}{\partial r^2} + \frac{2}{r}\frac{\partial}{\partial r}\right)[O_2] - Q \cdot a = 0 \quad (3c)$$

with reverse boundary conditions

$$[O_2](r = r_{plug}) = O_{2max}$$

$$\left.\frac{\partial [O_2]}{\partial r}\right|_{r=0} = 0$$

Finally, the expression for respiration rate Q (equation 2) can be substituted into equations 3a, b, and c to relate the diffusivity parameters to the physiological microbial constraints, with the whole expression nondimensionalized (38) to extract scaling parameters that intuitively relate the physical and physiological parameters to each other and simplify modeling. For modeling purposes, all spatial scales and concentrations are nondimensionalized using the following scaling factors (and introducing maintenance parameter g):

$$\{r^*, x^*\} \equiv \{r, x\} \cdot \sqrt{\frac{1}{D_{O_2}} \cdot \frac{\mu_{max} \cdot a}{k_{O_2} \cdot Y_{O_2}}}$$

$$[O_2^*] \equiv \frac{[O_2]}{k_{O_2}}$$

$$g \equiv \frac{Y_{O_2} \cdot P_{O_2}}{\mu_{max}}$$

This yields the following nondimensionalized equations for the different geometric scenarios:

$$\text{C:}\quad D_{O_2} \cdot \frac{\partial^2 [O_2]}{\partial x^2} - \left(\frac{\mu_{max}}{Y_{O_2}} \cdot \frac{[O_2]}{k_{O_2} + [O_2]} + P_{O_2}\right) \cdot a = 0$$

$$\frac{\partial^2 [O_2^*]}{\partial x^2} - \left(\frac{[O_2^*]}{1 + [O_2^*]} + g\right) = 0$$

and, similarly,

$$\text{B:}\quad \left(\frac{\partial^2 [O_2^*]}{\partial r^{*2}} + \frac{1}{r^*}\frac{\partial [O_2^*]}{\partial r^*}\right) - \left(\frac{[O_2^*]}{1 - [O_2^*]} + g\right) = 0$$

$$\text{A:}\quad \left(\frac{\partial^2 [O_2^*]}{\partial r^{*2}} + \frac{2}{r^*}\frac{\partial [O_2^*]}{\partial r^*}\right) - \left(\frac{[O_2^*]}{1 - [O_2^*]} + g\right) = 0$$

The parameters used to compute the scaling factors for the modeling (Table 2) are based on literature values compiled by various studies, with physiological parameters primarily derived from the compilation for *P. aeruginosa* by Kempes et al. (38). The main parameters adjusted in this study were the spatial scales (mucus thickness) and cell density, with additional oxygen diffusivity results presented in Fig. S3 in the supplemental material.

Diffusion was modeled in R using the ReacTran package (84), and steady-state concentrations were computed using the rootSolve package (85). A complete, documented copy of all scripts required to reproduce the modeling results and model fitting to collected data can be found in Text S1 and S2 in the supplemental material, where a link is provided to access this online information (hosted on Github).

SUPPLEMENTAL MATERIAL

Supplemental material for this article may be found at http://mbio.asm.org/lookup/suppl/doi:10.1128/mBio.00767-15/-/DCSupplemental.

Text S1, HTML file, 2.9 MB.
Text S2, HTML file, 1.8 MB.
Figure S1, EPS file, 0.03 MB.
Figure S2, PDF file, 0.1 MB.
Figure S3, PDF file, 0.3 MB.
Table S1, PDF file, 0.1 MB.
Table S2, PDF file, 0.01 MB.
Table S3, PDF file, 0.02 MB.
Table S4, DOCX file, 0.1 MB.
Table S5, DOCX file, 0.05 MB.

ACKNOWLEDGMENTS

This work was supported by NIH grant R01HL117328 and the Howard Hughes Medical Institute (HHMI). D.K.N. is an HHMI Investigator.

We thank Roberta Kato, Kyle McCallin, Carmen Reyes, and the entire pulmonary clinic team at Children's Hospital, Los Angeles, CA, for their support; Nathan Dalleska and the Caltech Environmental Analysis Center for instrumentation that benefitted this study; Chris Kempes for modeling advice; and members of the Newman laboratory and Unisense A/S for constructive feedback throughout this project.

REFERENCES

1. **Riordan JR, Rommens JM, Kerem B, Alon N, Rozmahel R, Grzelczak Z, Zielenski J, Lok S, Plavsic N, Chou JL.** 1989. Identification of the cystic fibrosis gene: cloning and characterization of complementary DNA. Science 245:1066–1073. http://dx.doi.org/10.1126/science.2475911.

2. **Boucher RC**. 2007. Airway surface dehydration in cystic fibrosis: pathogenesis and therapy. Annu Rev Med **58:**157–170. http://dx.doi.org/10.1146/annurev.med.58.071905.105316.
3. **Knowles MR, Boucher RC**. 2002. Mucus clearance as a primary innate defense mechanism for mammalian airways. J Clin Invest **109:**571–577. http://dx.doi.org/10.1172/JCI15217.
4. **Koch C, Høiby N**. 2000. Diagnosis and treatment of cystic fibrosis. Respiration **67:**239–247. http://dx.doi.org/10.1159/000029503.
5. **Chmiel JF, Davis PB**. 2003. State of the art: why do the lungs of patients with cystic fibrosis become infected and why can't they clear the infection? Respir Res **4:**8. http://dx.doi.org/10.1186/1465-9921-4-8.
6. **Koch C, Høiby N**. 1993. Pathogenesis of cystic fibrosis. Lancet **341:**1065–1069. http://dx.doi.org/10.1016/0140-6736(93)92422-P.
7. **Cystic Fibrosis Foundation**. 2014. Cystic Fibrosis Foundation Patient Registry 2013 annual data report. Cystic Fibrosis Foundation, Bethesda, MD.
8. **Hibbing ME, Fuqua C, Parsek MR, Peterson SB**. 2010. Bacterial competition: surviving and thriving in the microbial jungle. Nat Rev Microbiol **8:**15–25. http://dx.doi.org/10.1038/nrmicro2259.
9. **Smith EE, Buckley DG, Wu Z, Saenphimmachak C, Hoffman LR, D'Argenio DA, Miller SI, Ramsey BW, Speert DP, Moskowitz SM, Burns JL, Kaul R, Olson MV**. 2006. Genetic adaptation by *Pseudomonas aeruginosa* to the airways of cystic fibrosis patients. Proc Natl Acad Sci U S A **103:**8487–8492. http://dx.doi.org/10.1073/pnas.0602138103.
10. **Lyczak JB, Cannon CL, Pier GB**. 2002. Lung infections associated with cystic fibrosis. Clin Microbiol Rev **15:**194–222. http://dx.doi.org/10.1128/CMR.15.2.194-222.2002.
11. **Jorth P, Turner KH, Gumus P, Nizam N, Buduneli N, Whiteley M**. 2014. Metatranscriptomics of the human oral microbiome during health and disease. mBio **5:**e01012-14. http://dx.doi.org/10.1128/mBio.01012-14.
12. **Worlitzsch D, Tarran R, Ulrich M, Schwab U, Cekici A, Meyer KC, Birrer P, Bellon G, Berger J, Weiss T, Botzenhart K, Yankaskas JR, Randell S, Boucher RC, Döring G**. 2002. Effects of reduced mucus oxygen concentration in airway *Pseudomonas* infections of cystic fibrosis patients. J Clin Invest **109:**317–325. http://dx.doi.org/10.1172/JCI13870.
13. **Aanaes K, Rickelt LF, Johansen HK, von Buchwald C, Pressler T, Høiby N, Jensen PØ**. 2011. Decreased mucosal oxygen tension in the maxillary sinuses in patients with cystic fibrosis. J Cyst Fibros **10:**114–120. http://dx.doi.org/10.1016/j.jcf.2010.12.002.
14. **Kolpen M, Kühl M, Bjarnsholt T, Moser C, Hansen CR, Liengaard L, Kharazmi A, Pressler T, Høiby N, Jensen PØ**. 2014. Nitrous oxide production in sputum from cystic fibrosis patients with chronic *Pseudomonas aeruginosa* lung infection. PLoS One **9:**e84353. http://dx.doi.org/10.1371/journal.pone.0084353.
15. **Palmer KL, Aye LM, Whiteley M**. 2007. Nutritional cues control *Pseudomonas aeruginosa* multicellular behavior in cystic fibrosis sputum. J Bacteriol **189:**8079–8087. http://dx.doi.org/10.1128/JB.01138-07.
16. **Hunter RC, Klepac-Ceraj V, Lorenzi MM, Grotzinger H, Martin TR, Newman DK**. 2012. Phenazine content in the cystic fibrosis respiratory tract negatively correlates with lung function and microbial complexity. Am J Respir Cell Mol Biol **47:**738–745. http://dx.doi.org/10.1165/rcmb.2012-0088OC.
17. **Hunter RC, Asfour F, Dingemans J, Osuna BL, Samad T, Malfroot A, Cornelis P, Newman DK**. 2013. Ferrous iron is a significant component of bioavailable iron in cystic fibrosis airways. mBio **4:**e00557-13. http://dx.doi.org/10.1128/mBio.00557-13.
18. **Tate S, MacGregor G, Davis M, Innes JA, Greening AP**. 2002. Airways in cystic fibrosis are acidified: detection by exhaled breath condensate. Thorax **57:**926–929. http://dx.doi.org/10.1136/thorax.57.11.926.
19. **Newport S, Amin N, Dozor AJ**. 2009. Exhaled breath condensate pH and ammonia in cystic fibrosis and response to treatment of acute pulmonary exacerbations. Pediatr Pulmonol **44:**866–872. http://dx.doi.org/10.1002/ppul.21078.
20. **Xu KD, Stewart PS, Xia F, Huang C-T, McFeters GA**. 1998. Spatial physiological heterogeneity in *Pseudomonas aeruginosa* biofilm is determined by oxygen availability. Appl Environ Microbiol **64:**4035–4039.
21. **Hassett DJ**. 1996. Anaerobic production of alginate by *Pseudomonas aeruginosa*: alginate restricts diffusion of oxygen. J Bacteriol **178:**7322–7325.
22. **Alvarez-Ortega C, Harwood CS**. 2007. Responses of *Pseudomonas aeruginosa* to low oxygen indicate that growth in the cystic fibrosis lung is by aerobic respiration. Mol Microbiol **65:**153–165. http://dx.doi.org/10.1111/j.1365-2958.2007.05772.x.
23. **Glasser NR, Kern SE, Newman DK**. 2014. Phenazine redox cycling enhances anaerobic survival in *Pseudomonas aeruginosa* by facilitating generation of ATP and a proton-motive force. Mol Microbiol **92:**399–412. http://dx.doi.org/10.1111/mmi.12566.
24. **Yoon SS, Hennigan RF, Hilliard GM, Ochsner UA, Parvatiyar K, Kamani MC, Allen HL, DeKievit TR, Gardner PR, Schwab U, Rowe JJ, Iglewski BH, McDermott TR, Mason RP, Wozniak DJ, Hancock RE, Parsek MR, Noah TL, Boucher RC, Hassett DJ**. 2002. *Pseudomonas aeruginosa* anaerobic respiration in biofilms: relationships to cystic fibrosis pathogenesis. Dev Cell **3:**593–603. http://dx.doi.org/10.1016/S1534-5807(02)00295-2.
25. **Vander Wauven C, Piérard A, Kley-Raymann M, Haas D**. 1984. *Pseudomonas aeruginosa* mutants affected in anaerobic growth on arginine: evidence for a four-gene cluster encoding the arginine deiminase pathway. J Bacteriol **160:**928–934.
26. **Platt MD, Schurr MJ, Sauer K, Vazquez G, Kukavica-Ibrulj I, Potvin E, Levesque RC, Fedynak A, Brinkman FS, Schurr J, Hwang S-H, Lau GW, Limbach PA, Rowe JJ, Lieberman MA, Barraud N, Webb J, Kjelleberg S, Hunt DF, Hassett DJ**. 2008. Proteomic, microarray, and signature-tagged mutagenesis analyses of anaerobic *Pseudomonas aeruginosa* at pH 6.5, likely representing chronic, late-stage cystic fibrosis airway conditions. J Bacteriol **190:**2739–2758. http://dx.doi.org/10.1128/JB.01683-07.
27. **Filiatrault MJ, Wagner VE, Bushnell D, Haidaris CG, Iglewski BH, Passador L**. 2005. Effect of anaerobiosis and nitrate on gene expression in *Pseudomonas aeruginosa*. Infect Immun **73:**3764–3772. http://dx.doi.org/10.1128/IAI.73.6.3764-3772.2005.
28. **Van Alst NE, Picardo KF, Iglewski BH, Haidaris CG**. 2007. Nitrate sensing and metabolism modulate motility, biofilm formation, and virulence in *Pseudomonas aeruginosa*. Infect Immun **75:**3780–3790. http://dx.doi.org/10.1128/IAI.00201-07.
29. **Guss AM, Roeselers G, Newton IL, Young CR, Klepac-Ceraj V, Lory S, Cavanaugh CM**. 2011. Phylogenetic and metabolic diversity of bacteria associated with cystic fibrosis. ISME J **5:**20–29. http://dx.doi.org/10.1038/ismej.2010.88.
30. **Su S, Hassett DJ**. 2012. Anaerobic *Pseudomonas aeruginosa* and other obligately anaerobic bacterial biofilms growing in the thick airway mucus of chronically infected cystic fibrosis patients: an emerging paradigm or "Old Hat"? Expert Opin Ther Targets **16:**859–873. http://dx.doi.org/10.1517/14728222.2012.708025.
31. **Quinn RA, Lim YW, Maughan H, Conrad D, Rohwer F, Whiteson KL**. 2014. Biogeochemical forces shape the composition and physiology of polymicrobial communities in the cystic fibrosis lung. mBio **5:**e00956-13. http://dx.doi.org/10.1128/mBio.00956-13.
32. **Revsbech NP, Larsen LH, Gundersen J, Dalsgaard T, Ulloa O, Thamdrup B**. 2009. Determination of ultra-low oxygen concentrations in oxygen minimum zones by the STOX sensor. Limnol Oceanogr Methods **7:**371–381. http://dx.doi.org/10.4319/lom.2009.7.371.
33. **Jeroschewski P, Steuckart C, Kühl M**. 1996. An amperometric microsensor for the determination of H_2S in aquatic environments. Anal Chem **68:**4351–4357. http://dx.doi.org/10.1021/ac960091b.
34. **Kühl M, Steuckart C, Eickert G, Jeroschewski P**. 1998. A H_2S microsensor for profiling biofilms and sediments: application in an acidic lake sediment. Aquat Microb Ecol **15:**201–209. http://dx.doi.org/10.3354/ame015201.
35. **Kolpen M, Kragh KN, Bjarnsholt T, Line L, Hansen CR, Dalbøge CS, Hansen N, Kühl M, Høiby N, Jensen PØ**. 2015. Denitrification by cystic fibrosis pathogens—*Stenotrophomonas maltophilia* is dormant in sputum. Int J Med Microbiol **305:**1–10. http://dx.doi.org/10.1016/j.ijmm.2014.07.002.
36. **Kolpen M, Hansen CR, Bjarnsholt T, Moser C, Christensen LD, van Gennip M, Ciofu O, Mandsberg L, Kharazmi A, Döring G, Givskov M, Høiby N, Jensen PØ**. 2010. Polymorphonuclear leucocytes consume oxygen in sputum from chronic *Pseudomonas aeruginosa* pneumonia in cystic fibrosis. Thorax **65:**57–62. http://dx.doi.org/10.1136/thx.2009.114512.
37. **Babior BM, Curnutte JT, McMurrich BJ**. 1976. The particulate superoxide-forming system from human neutrophils. Properties of the system and further evidence supporting its participation in the respiratory burst. J Clin Invest **58:**989–996. http://dx.doi.org/10.1172/JCI108553.
38. **Kempes CP, Okegbe C, Mears-Clarke Z, Follows MJ, Dietrich LE**. 2014. Morphological optimization for access to dual oxidants in biofilms. Proc Natl Acad Sci U S A **111:**208–213. http://dx.doi.org/10.1073/pnas.1315521110.
39. **Stressmann FA, Rogers GB, Marsh P, Lilley AK, Daniels TW, Carroll MP, Hoffman LR, Jones G, Allen CE, Patel N, Forbes B, Tuck A, Bruce KD**. 2011. Does bacterial density in cystic fibrosis sputum increase prior to

pulmonary exacerbation? J Cyst Fibros **10:**357–365. http://dx.doi.org/10.1016/j.jcf.2011.05.002.
40. **Worthington EN, Tarran R.** 2011. Methods for ASL measurements and mucus transport rates in cell cultures, p 77–92. In Amaral MD, Kunzelmann K (ed), Cystic fibrosis. Humana Press, Totowa, NJ.
41. **Sims DE, Horne MM.** 1997. Heterogeneity of the composition and thickness of tracheal mucus in rats. Am J Physiol **273:**L1036–L1041.
42. **Luan X, Campanucci VA, Nair M, Yilmaz O, Belev G, Machen TE, Chapman D, Ianowski JP.** 2014. *Pseudomonas aeruginosa* triggers CFTR-mediated airway surface liquid secretion in swine trachea. Proc Natl Acad Sci U S A **111:**12930–12935. http://dx.doi.org/10.1073/pnas.1406414111.
43. **Cu Y, Saltzman WM.** 2009. Mathematical modeling of molecular diffusion through mucus. Adv Drug Deliv Rev **61:**101–114. http://dx.doi.org/10.1016/j.addr.2008.09.006.
44. **Harrison DEF.** 1972. Physiological effects of dissolved oxygen tension and redox potential on growing populations of micro-organisms. J Appl Chem **22:**417–440. http://dx.doi.org/10.1002/jctb.5020220311.
45. **Stolper DA, Revsbech NP, Canfield DE.** 2010. Aerobic growth at nanomolar oxygen concentrations. Proc Natl Acad Sci U S A **107:**18755–18760. http://dx.doi.org/10.1073/pnas.1013435107.
46. **Faust K, Sathirapongsasuti JF, Izard J, Segata N, Gevers D, Raes J, Huttenhower C.** 2012. Microbial co-occurrence relationships in the human microbiome. PLoS Comput Biol **8:**e1002606. http://dx.doi.org/10.1371/journal.pcbi.1002606.
47. **Teske AP.** 2012. Tracking microbial habitats in subseafloor sediments. Proc Natl Acad Sci U S A **109:**16756–16757. http://dx.doi.org/10.1073/pnas.1215867109.
48. **Yu Z, Yang J, Amalfitano S, Yu X, Liu L.** 2014. Effects of water stratification and mixing on microbial community structure in a subtropical deep reservoir. Sci Rep **4:**5821. http://dx.doi.org/10.1038/srep05821.
49. **Stoeck T, Filker S, Edgcomb V, Orsi W, Yakimov MM, Pachiadaki M, Breiner H-W, LaCono V, Stock A.** 2014. Living at the limits: evidence for microbial eukaryotes thriving under pressure in deep anoxic, hypersaline habitats. Adv Ecol **2014:**532687.
50. **Dick GJ, Anantharaman K, Baker BJ, Li M, Reed DC, Sheik CS.** 2013. The microbiology of deep-sea hydrothermal vent plumes: ecological and biogeographic linkages to seafloor and water column habitats. Front Microbiol **4:**124. http://dx.doi.org/10.3389/fmicb.2013.00124.
51. **Stumm W, Morgan JJ.** 1996. Aquatic chemistry: chemical equilibria and rates in natural waters. Wiley, New York, NY.
52. **de Lacy Costello BPJ, Ewen RJ, Ratcliffe NM.** 2008. A sensor system for monitoring the simple gases hydrogen, carbon monoxide, hydrogen sulfide, ammonia and ethanol in exhaled breath. J Breath Res **2:**037011. http://dx.doi.org/10.1088/1752-7155/2/3/037011.
53. **Ruiz R, Hartman TG, Karmas K, Lech J, Rosen RT.** 1993. Breath analysis of garlic-borne phytochemicals in human subjects, p 102–119. In Food phytochemicals for cancer prevention I. American Chemical Society, Washington, DC.
54. **Pysanenko A, Španěl P, Smith D.** 2008. A study of sulfur-containing compounds in mouth- and nose-exhaled breath and in the oral cavity using selected ion flow tube mass spectrometry. J Breath Res **2:**046004. http://dx.doi.org/10.1088/1752-7155/2/4/046004.
55. **Wang Y, Newman DK.** 2008. Redox reactions of phenazine antibiotics with ferric (hydr)oxides and molecular oxygen. Environ Sci Technol **42:**2380–2386. http://dx.doi.org/10.1021/es702290a.
56. **Ragsdale SW, Pierce E.** 2008. Acetogenesis and the Wood-Ljungdahl pathway of CO_2 fixation. Biochim Biophys Acta **1784:**1873–1898. http://dx.doi.org/10.1016/j.bbapap.2008.08.012.
57. **Gibson GR, Cummings JH, Macfarlane GT.** 1991. Growth and activities of sulphate-reducing bacteria in gut contents of healthy subjects and patients with ulcerative colitis. FEMS Microbiol Lett **86:**103–111. http://dx.doi.org/10.1111/j.1574-6968.1991.tb04799.x.
58. **Lim YW, Schmieder R, Haynes M, Willner D, Furlan M, Youle M, Abbott K, Edwards R, Evangelista J, Conrad D, Rohwer F.** 2013. Metagenomics and metatranscriptomics: windows on CF-associated viral and microbial communities. J Cyst Fibros **12:**154–164. http://dx.doi.org/10.1016/j.jcf.2012.07.009.
59. **Hampton TH, Green DM, Cutting GR, Morrison HG, Sogin ML, Gifford AH, Stanton BA, O'Toole GA.** 2014. The microbiome in pediatric cystic fibrosis patients: the role of shared environment suggests a window of intervention. Microbiome **2:**14. http://dx.doi.org/10.1186/2049-2618-2-14.
60. **Price KE, Hampton TH, Gifford AH, Dolben EL, Hogan DA, Morrison HG, Sogin ML, O'Toole GA.** 2013. Unique microbial communities persist in individual cystic fibrosis patients throughout a clinical exacerbation. Microbiome **1:**27. http://dx.doi.org/10.1186/2049-2618-1-27.
61. **Hespell RB, Canale-Parola E.** 1971. Amino acid and glucose fermentation by *Treponema denticola*. Arch Mikrobiol **78:**234–251. http://dx.doi.org/10.1007/BF00424897.
62. **Mendes-Ferreira A, Barbosa C, Inês A, Mendes-Faia A.** 2010. The timing of diammonium phosphate supplementation of wine must affects subsequent H2S release during fermentation. J Appl Microbiol **108:**540–549. http://dx.doi.org/10.1111/j.1365-2672.2009.04457.x.
63. **Kadota H, Ishida Y.** 1972. Production of volatile sulfur compounds by microorganisms. Annu Rev Microbiol **26:**127–138. http://dx.doi.org/10.1146/annurev.mi.26.100172.001015.
64. **Kiene RP, Visscher PT.** 1987. Production and fate of methylated sulfur compounds from methionine and dimethylsulfoniopropionate in anoxic salt marsh sediments. Appl Environ Microbiol **53:**2426–2434.
65. **Shatalin K, Shatalina E, Mironov A, Nudler E.** 2011. H_2S: a universal defense against antibiotics in bacteria. Science **334:**986–990. http://dx.doi.org/10.1126/science.1209855.
66. **Filkins LM, Graber JA, Olson DG, Dolben EL, Lynd LR, Bhuju S, O'Toole GA.** 2015. Co-culture of *Staphylococcus aureus* with *Pseudomonas aeruginosa* drives *S. aureus* towards fermentative metabolism and reduced viability in a cystic fibrosis model. J Bacteriol http://dx.doi.org/10.1128/JB.00059-15.
67. **Behrends V, Ryall B, Zlosnik JE, Speert DP, Bundy JG, Williams HD.** 2013. Metabolic adaptations of *Pseudomonas aeruginosa* during cystic fibrosis chronic lung infections. Environ Microbiol **15:**398–408. http://dx.doi.org/10.1111/j.1462-2920.2012.02840.x.
68. **Weinrick B, Dunman PM, McAleese F, Murphy E, Projan SJ, Fang Y, Novick RP.** 2004. Effect of mild acid on gene expression in *Staphylococcus aureus*. J Bacteriol **186:**8407–8423. http://dx.doi.org/10.1128/JB.186.24.8407-8423.2004.
69. **Henry-Stanley MJ, Hess DJ, Wells CL.** 2014. Aminoglycoside inhibition of *Staphylococcus aureus* biofilm formation is nutrient dependent. J Med Microbiol **63:**861–869. http://dx.doi.org/10.1099/jmm.0.068130-0.
70. **De la Fuente-Núñez C, Reffuveille F, Fernández L, Hancock RE.** 2013. Bacterial biofilm development as a multicellular adaptation: antibiotic resistance and new therapeutic strategies. Curr Opin Microbiol **16:**580–589. http://dx.doi.org/10.1016/j.mib.2013.06.013.
71. **Gadalla MM, Snyder SH.** 2010. Hydrogen sulfide as a gasotransmitter. J Neurochem **113:**14–26. http://dx.doi.org/10.1111/j.1471-4159.2010.06580.x.
72. **Zanardo RC, Brancaleone V, Distrutti E, Fiorucci S, Cirino G, Wallace JL.** 2006. Hydrogen sulfide is an endogenous modulator of leukocyte-mediated inflammation. FASEB J **20:**2118–2120. http://dx.doi.org/10.1096/fj.06-6270fje.
73. **Lo Faro ML, Fox B, Whatmore JL, Winyard PG, Whiteman M.** 2014. Hydrogen sulfide and nitric oxide interactions in inflammation. Nitric Oxide **41:**38–47. http://dx.doi.org/10.1016/j.niox.2014.05.014.
74. **Chen Y-H, Yao W-Z, Geng B, Ding Y-L, Lu M, Zhao M-W, Tang C-S.** 2005. Endogenous hydrogen sulfide in patients with COPD. Chest **128:**3205–3211. http://dx.doi.org/10.1378/chest.128.5.3205.
75. **Kamboures MA, Blake DR, Cooper DM, Newcomb RL, Barker M, Larson JK, Meinardi S, Nussbaum E, Rowland FS.** 2005. Breath sulfides and pulmonary function in cystic fibrosis. Proc Natl Acad Sci U S A **102:**15762–15767. http://dx.doi.org/10.1073/pnas.0507263102.
76. **Tian M, Wang Y, Lu YQ, Yan M, Jiang YH, Zhao DY.** 2012. Correlation between serum H_2S and pulmonary function in children with bronchial asthma. Med Mol Rep **6:**335–338. http://dx.doi.org/10.3892/mmr.2012.904.
77. **Chung KF.** 2014. Hydrogen sulfide as a potential biomarker of asthma. Expert Rev Respir Med **8:**5–13. http://dx.doi.org/10.1586/17476348.2014.856267.
78. **Wu CHK.** 2013. The role of hydrogen sulphide in lung diseases. Biosci Horiz **6:**hzt009. http://dx.doi.org/10.1093/biohorizons/hzt009.
79. **Garcia G.** 1993. Oxygen solubility in seawater—better fitting equations (vol 37, p 1308, 1992). Limnol Oceanogr **38:**656.
80. **Revsbech NP.** 1989. An oxygen microsensor with a guard cathode. Limnol Oceanogr **34:**474–478. http://dx.doi.org/10.4319/lo.1989.34.2.0474.
81. **Andersen K, Kjær T, Revsbech NP.** 2001. An oxygen insensitive microsensor for nitrous oxide. Sens Actuators B Chem **81:**42–48. http://dx.doi.org/10.1016/S0925-4005(01)00924-8.
82. **Thomas RC.** 1979. Ion-sensitive intracellular microelectrodes: how to make and use them. Academic Press, London, United Kingdom.

83. **Pang H, Zhang TC**. 1998. Fabrication of redox potential microelectrodes for studies in vegetated soils or biofilm systems. Environ Sci Technol **32:** 3646–3652. http://dx.doi.org/10.1021/es980024u.
84. **Soetaert K, Meysman F**. 2012. Reactive transport in aquatic ecosystems: rapid model prototyping in the open source software R. Environ Model Softw **32:**49–60. http://dx.doi.org/10.1016/j.envsoft.2011.08.011.
85. **Soetaert K, Herman P**. 2009. Using R as a simulation platform, p 372. In A practical guide to ecological modelling. Springer, Heidelberg, Germany.
86. **Stewart PS**. 2003. Diffusion in biofilms. J Bacteriol **185:**1485–1491. http://dx.doi.org/10.1128/JB.185.5.1485-1491.2003.
87. **Saldeña TA, Saraví FD, Hwang HJ, Cincunegui LM, Carra GE**. 2000. Oxygen diffusive barriers of rat distal colon: role of subepithelial tissue, mucosa, and mucus gel layer. Dig Dis Sci **45:**2108–2114. http://dx.doi.org/10.1023/A:1026411118033.
88. **Beyenal H, Chen SN, Lewandowski Z**. 2003. The double substrate growth kinetics of Pseudomonas aeruginosa. Enzyme Microb Technol **32:**92–98. http://dx.doi.org/10.1016/S0141-0229(02)00246-6.
89. **Morel FMM, Hering JG**. 1993. Principles and applications of aquatic chemistry. John Wiley & Sons, Inc, Hoboken, NJ.
90. **Bujanover Y, Peled Y, Blau H, Yahav J, Katzenelson D, Gilat T**. 1987. Methane production in patients with cystic fibrosis. J Pediatr Gastroenterol Nutr **6:**377–380. http://dx.doi.org/10.1097/00005176-198705000-00013.
91. **Catalán MA, Scott-Anne K, Klein MI, Koo H, Bowen WH, Melvin JE**. 2011. Elevated incidence of dental caries in a mouse model of cystic fibrosis. PLoS One **6:**e16549. http://dx.doi.org/10.1371/journal.pone.0016549.
92. **Zmantar T, Kouidhi B, Miladi H, Mahdouani K, Bakhrouf A**. 2010. A microtiter plate assay for *Staphylococcus aureus* biofilm quantification at various pH levels and hydrogen peroxide supplementation. New Microbiol **33:**137–145.